Optimal kinematics of supercoiled filaments

Francesca Maggioni[§], Florian A. Potra[*], Marida Bertocchi[§]

Abstract. New kinematics of supercoiling of closed filaments as solutions of the elastic energy minimization are proposed. The analysis is based on the thin rod approximation of linear elastic theory, under conservation of self-linking number with elastic energy evaluated by means of bending contribution, due to curvature effects and torsional influence due to torsion and intrinsic twist. The deformation energy of the system is required to be monotonically decreasing in time, favoring the folding process for fixed initial condition given by a critical twist value chosen to generate writhing instability [9]. Constraints to ensure the inextensibility of the filament are also included. Time evolution functions are described by means of piecewise polynomial transformations based on cubic B-spline and Hermite spline functions. We impose proper constraints so that the transformation is globally C^2 and smoothing penalties on norm and curvature are also included. In contrast with traditional interpolation, values at grids points of the evolution functions are considered as the unknowns in a non-linear optimization problem. We show how the coiling process is associated with conversion of mean twist energy into bending energy through the passage by an inflexional configuration in relation to geometric characteristics of the filament evolution. These results shed new light on the folding mechanism and associated energy contents and find useful applications in the general context of structural genomics and proteomics.

Key words: Kinematics of curves, writhing, DNA supercoiling, twist, deformation energy, non-linear optimization, cubic B-spline function.

Mathematics Subject Classification (2010):

1 Introduction

In this paper we propose a new model to investigate the supercoiling process of closed filaments in the context of elastic filaments. The analysis is based on the thin rod approximation of linear elastic theory, under conservation of self-linking number with elastic energy evaluated

[§]Department of Mathematics, Statistic, Computer Science and Applications, Bergamo University, Via dei Caniana 2, Bergamo 24127, Italy. e-mail: francesca.maggioni@unibg.it, marida.bertocchi@unibg.it

[*]Department of Mathematics & Statistic, University of Maryland, Baltimore County, Baltimore, MD 21250, U.S.A. e-mail: potra@umbc.edu

by means of bending contribution, due to curvature effects and torsional influence due to torsion and intrinsic twist.

Kinematics of coils formation has been already analysed in [12] and [17] by means of a set of governing equations which prescribed the time-dependent evolutions of curves generated by epicycloids and hypocycloids and compared in terms of geometric and energetic aspects. It was shown that high degree of coiling may be achieved at relatively low energy costs through appropriate folding and twist distribution, and independently from the number of coils formed. Hoverer, this class of curve evolutions, represents just one-parameter group embedded in an infinite-dimensional family of kinematically possible deformations; there may well exist other paths in the space of curve deformations that may be energetically preferable: this will be addressed in this paper in the context of elastic filaments.

We propose to extend the model by determining the time-dependence curves with deformation energy monotonically decreasing in time, favoring folding. Initial condition given by a critical twist value are chosen in agreement with analytical results in the context of elastic rod theory (see [13], [26], [9]) to generate writhing instability. The model includes constraints to ensure the inextensibility of the filament. Time evolution functions are described by means of piecewise polynomial transformations based on cubic B-spline and Hermite spline functions. We impose proper constraints so that the transformation is globally C^2 in the sense that the evolution itself with the first and second order derivatives are continuous. Smoothing penalties on norm and curvature of time evolution functions are also included. Moreover, in contrast with traditional interpolation, where values at grids points (vertices) have to match some given values, we consider the values of the evolution functions at grid points as part of the unknowns in a non-linear optimization problem. We show how the coiling process is associated with conversion of mean twist energy into bending energy through the passage by an inflexional configuration in relation to geometric characteristics of the filament evolution such as writhing number, normalized total curvature and twist in terms of its contributions from normalized total torsion and intrinsic twist.

The model can be considered to explore the phenomenon of writhing or supercoiled instability observed in twisting elastic filaments in the context of elastic rod theory. The energetics of the circular uniformly twisted equilibrium configuration were analyzed by Michell in 1889 [13] and rediscovered by Zajac in 1962 [26] (see [9]) and more recently in [3] and [11] in elastic model for DNA, indicating that for a certain critical total twist this configuration no longer has minimum energy. For small values of the twist, the twisted ring is stable and conversely, for sufficiently high twist, the elastic ring become unstable and will start writhing out of the plane. The stability of twisted elastic rings became of interest also in biophysics when it was first realized that geometric and topological characterizations of curves could be of importance to understand DNA configurations [8].

While the static theory of elastic rods is classical and well studied [24]-[20][21], their dynamics have received attention particularly with regards to computational methods [10]. During the past year, a variety of diverse and complementary approaches have been presented, offering new physical and biological insights into fundamental functional processes of DNA. Analytical approaches have probed deeper into the effects of entropy and thermal fluctuations on

DNA structure and on various topological constraints induced by DNA-binding proteins. New kinetic approaches - by molecular, Langevin, and Brownian dynamics, as well as extensions of elastic-rod theory - have begun to offer dynamic information associated with supercoiling [18]-[19].

Supercoiling phenomena revests a key role in DNA. Many DNA's in bacteria, viruses and mitochondrion are found in the form of loops. The looped DNA's often wind in space to take intricate structures, in which case they are said to be supercoiled [4]. It is an interesting fact that a large portion of DNA's exhibit some form of supercoiling in at least one stage of their life cycles.

Geometric information also plays a crucial role in relation to topology [22]-[6]. DNA topology in vivo is extremely diverse. In bacteria, circular plasmids are condensed by supercoiling the DNA into highly writhed superhelical structures. Families of topoisomerase and gyrase enzymes alter the level of supercoiling by transiently introducing single or double strand breaks and changing the number of times the two strand of the duplex are wrapped around each other. Variation in DNA topology influences promoter activity and is consequently involved in the regulation of gene expression and replication.

The paper is organized as follows: in the next section we recall kinematics models of multiple coiling analyzed in [12] and [17] where the time dependence was prescribed. Section 3 discusses geometric and topological measures of filament coiling, folding and twist and the deformation energy associated to the coiling process by using linear elastic theory of thin rod approximation. Section 4 presents the model and section 5 the methodology adopted to solve it in terms of cubic B-spline and Hermite spline functions. Numerical results in the case of single coil formation are presented in Section 6 analyzing geometric characteristics of the filament evolution in relation to the occurrence of an inflexional configuration. Section 7 concludes the paper.

2 Kinematics of supercoiling

The filament folding mechanism is investigated by improving simple kinematic models of time-evolution of an inextensible, closed curve $\mathcal{C}$ in three-dimensional space, introduced in [12] and [17]. The curve is given by a smooth (at least C^3), simple (i.e. non-self-intersecting), closed curve with parametric equation $\mathbf{X} = \mathbf{X}(\xi, t)$ in $\mathbb{R}^3$, where $\xi \in [0, 2\pi]$ parametrizes the points along the curve and where t is a kinematic parameter (typically the time).
The time-dependent curve $\mathbf{X} = \mathbf{X}(\xi, t)$ is then described by the following model:

$$\mathbf{X} = \mathbf{X}(\xi, t) \ : \quad \begin{cases} x = [a_1(t)\cos(n_1\xi) + a_2(t)\cos(n_2\xi)] \\ y = [a_3(t)\sin(n_1\xi) + a_4(t)\sin(n_2\xi)] \\ z = [a_5(t)\sin(\xi)] \end{cases} , \tag{1}$$

where the integer parameters $n_2 > n_1 > 0$ control the number of coils produced and $a_i(t),\ i = 1, \ldots, 5$ are time-dependent functions.

In order to ensure inextensibility, each $\mathbf{X}$-component is normalized by the length function:

$$l(t) = \frac{1}{2\pi}\int_0^{2\pi}\left[\left(\frac{\partial x}{\partial \xi}\right)^2 + \left(\frac{\partial y}{\partial \xi}\right)^2 + \left(\frac{\partial z}{\partial \xi}\right)^2\right]^{1/2} \mathrm{d}\xi \ , \tag{2}$$

and eqs. (1) is then replaced by the following:

$$\mathbf{X} = \mathbf{X}(\xi, t) \ : \quad \begin{cases} x = \left[a_1(t)\cos\left(n_1\xi\right) + a_2(t)\cos\left(n_2\xi\right)\right]/l(t) \\ y = \left[a_3(t)\sin\left(n_1\xi\right) + a_4(t)\sin\left(n_2\xi\right)\right]/l(t) \\ z = \left[a_5(t)\sin\left(\xi\right)\right]/l(t) \end{cases} . \tag{3}$$

For simplicity, in [12] and [17], constant and linear time dependence prescription has been considered and the time-dependent functions $a_i(t),\ i = 1, \ldots, 5$ have been chosen as follows:

$$a_1(t) = a_3(t) = 1, \quad a_2(t) = a_4(t) = a_5(t) = \pm t \ ,$$

referring to epicycloid or hypocycloid type of curve in relation to the corresponding type of plane curve in the $xy-$projection. With the above prescription eqs. (3) describe the time evolution of closed curves with initial condition ($t = 0$) chosen in order to originate from a plane circle of length $L = 2\pi$, and to evolve to form single coiled (see Fig. 1) or supercoiled configurations (see Fig. 2 in the case of 5 coils). The coil is produced by folding the curve in space, through the development of a loop region that gives rise to the full coil. This type of deformation is known as *Reidemeister type I move* and it leaves the topology of the curve unchanged.

Conversely, an appropriate time-dependent prescription should be dictated by the specific physical process considered. The particular time-dependent class of curves chosen in [12] and [17] to represent the coil transition are in fact just one-parameter groups embedded in an infinite-dimensional family of kinematically possible deformations; there may well exist other paths in the space of curve deformations that may be energetically preferable: this will be addressed in this paper in the context of elastic filaments. We will determine the time-dependent functions $a_i(t)$, $i = 1, \ldots, 5$ such that the curve deformations (3) are energetically preferred in terms of elastic energy functional.

3 Measures and energetics of supercoiling

The total amount of filament coiling, folding and twist are quantified by global geometric quantities such as the normalized total curvature, the writhing number and twist. Let $c = c(\xi, t)$ denote the curvature and $\tau = \tau(\xi, t)$ the torsion of the curve $\mathbf{X}(t)$ through the standard Frenet-Serret formulae at time t.
Coiling is naturally measured by the *normalized total curvature* $K(t)$, given by

$$K(t) := \frac{1}{2\pi}\oint_{\mathcal{C}} c(\xi, t)\|\mathbf{X}'(\xi, t)\|\,\mathrm{d}\xi \ , \tag{4}$$

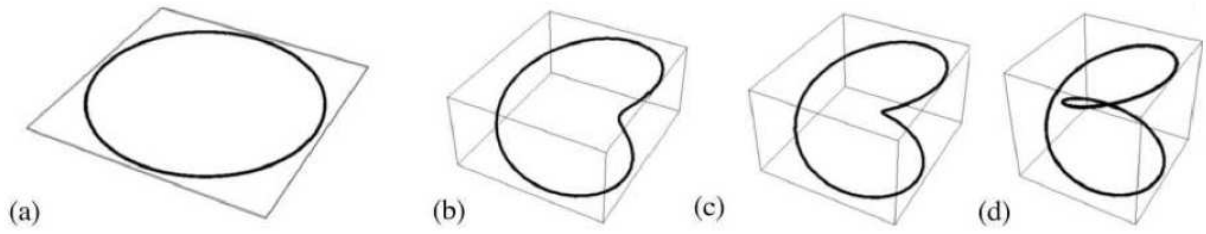

Figure 1: Single coil formation generated by eqs. (3) for $n_1 = 1$ and $n_2 = 2$ and kinematic parameters $a_1(t) = a_3(t) = 1$, $a_2(t) = a_4(t) = -t$ and $a_5(t) = t$. The initial circular configuration (a) writhes and folds in space (b)-(c) to produce the final coil (d).

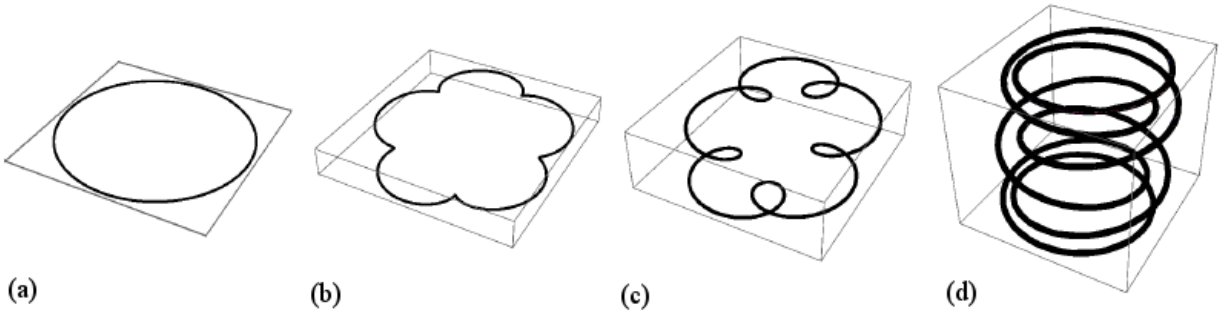

Figure 2: Five coils formation generated by eqs. (3) for $n_1 = 1$ and $n_2 = 6$ and kinematic parameters $a_1(t) = a_3(t) = 1$, $a_2(t) = a_4(t) = -t$ and $a_5(t) = t$. The initial circular configuration (a) writhes and folds in space in 5 different places (b)-(c) to produce 5 final coils (d).

where prime denotes derivative with respect to ξ and the factor $\|\mathbf{X}'(\xi,t)\|$ measures the length of the tangent vector $\mathbf{X}'(\xi,t)$ of the curve $\mathbf{X}$ at ξ at time t.

An important descriptor of *supercoiling* is given by the *writhing number* $Wr(t)$ [8], defined by

$$Wr(t) := \frac{1}{4\pi} \oint_{\mathcal{C}(t)} \oint_{\mathcal{C}(t)} \frac{\hat{\mathbf{t}}(\xi,t) \times \hat{\mathbf{t}}(\xi^*,t) \cdot [\mathbf{X}(\xi,t) - \mathbf{X}(\xi^*,t)]}{|\mathbf{X}(\xi,t) - \mathbf{X}(\xi^*,t)|^3} \|\mathbf{X}'(\xi,t)\| \|\mathbf{X}'(\xi^*,t)\| \, \mathrm{d}\xi \mathrm{d}\xi^* \ , \quad (5)$$

where $\mathbf{X}(\xi,t)$ and $\mathbf{X}(\xi^*,t)$ denote two points on the axis for any pair $\{\xi,\xi^*\} \in [0,2\pi]$, $\hat{\mathbf{t}}(\xi,t) := \mathbf{X}'(\xi,t)/\|\mathbf{X}'(\xi,t)\|$ is the unit tangent to $\mathcal{C}(t)$ at ξ at time t and the integration is performed twice on the same curve $\mathcal{C}(t)$.

A simple geometric interpretation of Wr is in terms of the algebraic sum of positive and negative crossings of the plane projection of the curve $\mathcal{C}(t)$.

Suppose to view the curve $\mathcal{C}(t)$ along the viewing direction $\boldsymbol{\nu}$: let $n_+(\boldsymbol{\nu}, t)$ be the number of positive crossings and $n_-(\boldsymbol{\nu}, t)$ the number of negative crossing of the projected curve at time t, where we have assigned a positive or negative sign to each intersection site of the oriented diagram according to the orientation of the curve $\mathcal{C}(t)$.
Then:

$$Wr(t) =< n_+(\boldsymbol{\nu}, t) - n_-(\boldsymbol{\nu}, t) > , \tag{6}$$

where the angular brackets denote averaging over all directions $\boldsymbol{\nu}$ of projection (see [8]). The writhing number depends only on the *geometry* of the curve $\mathcal{C}(t)$, it is invariant under rigid motions or dilations of the space containing the curve, its sign changes by reflection in a plane, it changes continuously under continue deformations of $\mathcal{C}(t)$ over time and jumps by ± 2 as the curve passes through itself.

A measure of the *winding* of the infinitesimal fibres around $\mathcal{C}(t)$ is given by the *total twist number* $Tw(t)$ defined by:

$$Tw(t) = \frac{1}{2\pi} \oint_{\mathcal{C}(t)} \Omega(\xi, t) \|\mathbf{X}'(\xi, t)\| \, \mathrm{d}\xi = \frac{1}{2\pi} \int_{\mathcal{C}(\mathrm{t})} \left(\hat{\mathbf{N}}'(\xi, \mathrm{t}) \times \hat{\mathbf{N}}(\xi, \mathrm{t}) \right) \cdot \hat{\mathbf{t}}(\xi, \mathrm{t}) \, \|\mathbf{X}'(\xi, \mathrm{t})\| \mathrm{d}\xi \ , \tag{7}$$

where $\Omega = \left(\hat{\mathbf{N}}' \times \hat{\mathbf{N}} \right) \cdot \hat{\mathbf{t}}$ is the *angular twist rate* and $\hat{\mathbf{N}}' = \dfrac{\mathrm{d}\hat{\mathbf{N}}}{\mathrm{d}\xi}$.
Tw can be decomposed as the sum of the normalized total torsion $\mathcal{T}(t)$ and the intrinsic twist $\mathcal{N}(t)$ of the fibers *around* $\mathcal{C}(t)$ as follows:

$$Tw(t) := \frac{1}{2\pi} \oint_{\mathcal{C}(t)} \tau(\xi, t) \|\mathbf{X}'(\xi, t)\| \, \mathrm{d}\xi + \frac{1}{2\pi} [\Theta(\mathrm{t})]_{\mathcal{F}} = \mathcal{T}(\mathrm{t}) + \mathcal{N}(\mathrm{t}) \ , \tag{8}$$

where $\Theta(t)$ is the total number of turns of twist at time t. For simplicity we take the fibers to be closed curves uniformly wound about $\mathcal{C}$, then $\mathcal{N}$ is an integer.
Tw is invariant under rigid motions or dilations of the space containing the filament, it is *additive* and it changes continuously, without any jump, under deformation of the filament in time, even if the axis curve passes through itself.

Note that K, Wr and $\mathcal{T}$ depend only on the geometry of the filament axis, whereas the total twist Tw and the intrinsic twist $\mathcal{N}$ depend also on the distribution of the filament fibers.

According to the well-known Calugareanu-White formula ([5] and [25]), the sum of $Wr(t)$ and $Tw(t)$ provides a topological invariant called *linking number* Lk:

$$Lk = Wr(t) + Tw(t) \ , \tag{9}$$

which establishes a conservation of topology during the folding process through a continuous change of the filament geometry and conversion of twist Tw in Wr. This will be crucial for the energy of the system, characterized by a transfer of torsional energy to bending energy [16].

We analyze the energetics of folding by adopting the linear elastic theory for a uniformly homogeneous and isotropic filament of circular cross section and inextensible length.

The elastic characteristics are specified by the bending stiffness K_b and the torsional stiffness K_t of the filament which can be estimated from experimental measurements and with ratio $\chi = K_b/K_t$ which lies between 1 (compressible material) and 1.5 (incompressible) with metals around 5/4. DNA filaments may present higher values of twist to bending rigidity.

The associated deformation energy can then be described in terms of bending and twisting components:

$$E(t) = E_b(t) + E_t(t) = \frac{1}{2}\oint_{\mathcal{C}} [K_b(c(\xi,t))^2 + K_t(\Omega(\xi,t) - \Omega_0)^2] \|\mathbf{X}'(\xi,t)\| \, \mathrm{d}\xi \ , \tag{10}$$

where we assumed zero natural angular twist rate Ω_0 of the filament fibers. The bending energy $E_b(t)$ is due to curvature effects and the torsional energy $E_t(t)$ is due to torsion and intrinsic twist.

Typically it is supposed that the twist rate Ω is constant along the filament ($\Omega = \Omega_c$, relaxed state) and then the term $E_t(t)$ can be replaced by the *mean twist* energy $E_{tw}(t)$, given by

$$E_{tw}(t) := E_t|_{\Omega_c}(t) = \frac{K_t L}{2}(\Omega_c)^2 = \pi K_t (Lk - Wr(t))^2 \ . \tag{11}$$

This simplication allows to base all computation only on the geometry of the curve $\mathbf{X}$.
Normalizing each term with respect to a reference configuration energy E_0, associated to the circular configuration of radius $R_0 = c_0^{-1} = 1$ and zero twist $E_0 = \pi K_b$, the relative total energy takes the form:

$$\tilde{E}(t) = \tilde{E}_b(t) + \tilde{E}_{tw}(t) = \frac{1}{2\pi}\oint_{\mathcal{C}} (c(\xi,t))^2 \|\mathbf{X}'(\xi)\| \, \mathrm{d}\xi + \frac{(\mathrm{Lk} - \mathrm{Wr(t)})^2}{\chi} \ . \tag{12}$$

4 Coiling formation under elastic energy minimization

In case the coiling process is favored, the total energy $\tilde{E}(t)$ (12) is monotonic decreasing in time, attaining at $t = 0$ its largest value that is going to be relaxed. From (12) we get:

$$\tilde{E}(0) = 1 + \frac{Lk^2}{\chi} \ , \tag{13}$$

which quadratically depends by Lk.

In [17] for prescribed time evolution, such a monotonically decreasing behavior was obtained by changing the linking number Lk (or twist Tw since at $t = 0$ $Wr = 0$) of the filament structure. For the single coil case, it was found that with $Lk \geq 9$, the total energy always decreases, independently of χ, hence favoring coiling.

However, it should be admitted here that the imposed condition on initial to provide spontaneous coiling is sufficient, but not necessary.

In addition, the critical twist value Tw_c to generate the *writhing instability* where the (unstable) twisted ring folds out of the plane, has been identified by Michell in 1889 [13] and

rediscovered by Zajac in 1962 [26] (see [9]) and more recently in [3] and [11] in elastic model for DNA:

$$Tw_c = \frac{\sqrt{3}}{R}\chi \ . \tag{14}$$

This means that a circular filament of unitary radius R becomes unstable when it has been twisted by about two full turns (with limits 1.73 to 2.6 corresponding to χ between 1 and 1.5).

This important information will be taken into account in the following model which determines the time-dependent functions $a_i(t)$, $i = 1, \ldots, 5$ in eq. (3), such that the coiling process is energetically preferred in terms of elastic deformation energy.
The problem is modelled as follows:

$$\min_{a_i(t)\ i=1,\ldots,5} \quad \int_{t_0}^{t_{fin}} \tilde{E}(a_i(t))\mathrm{d}t, \tag{15}$$

$$s.t. \quad \frac{\mathrm{d}}{\mathrm{d}t}\tilde{E}(a_i(t)) \leq 0, \qquad i = 1, \ldots, 5, \tag{16}$$

$$\tilde{E}(a_i(t_0)) = \tilde{E}_0, \qquad i = 1, \ldots, 5, \tag{17}$$

$$l(a_i(t)) = 2\pi, \qquad i = 1, \ldots, 5, \qquad t \in [t_0, t_{fin}]\,, \tag{18}$$

where the objective function represents the minimization along the time interval $[t_0, t_{fin}]$ of normalized total energy $\tilde{E}(a_i(t)) = \tilde{E}_b(a_i(t)) + \tilde{E}_{tw}(a_i(t))$ with respect to the time-dependent functions $a_i(t)$, $i = 1, \ldots, 5$. Problem (15)-(18) finds the state variables $a_i(t)$ such that the total elastic energy $\tilde{E}$ is minimimized in $[t_0, t_{fin}]$, it is monotonic decreasing in time (16) favoring coiling, it satisfies the initial condition (17) corresponding to a circle of unitary radius and, because of the inextensibility assumption, the length $l(t)$ of the filament is kept constant (18).

5 Numerical methods

Problem (15)-(18) is solved by considering the corresponding discrete version obtained dividing the time interval $[t_0, t_{fin}] = [t_0, t_F]$ into F equidistant sub-intervals of width $q = \frac{t_{fin} - t_0}{F}$:

$$\min_{a_i(t_f)\ i=1,\ldots,5} \quad q\left[\frac{\tilde{E}(t_0) + \tilde{E}(t_F)}{2} + \sum_{f=1}^{F-1} \tilde{E}(a_i(t_f))\right] + \gamma \sum_{f=0}^{F} p(t_f) + \mu \sum_{f=1}^{F-1} h(t_f) \tag{19}$$

$$s.t. \ \ \tilde{E}(a_i(t_f)) \geq \tilde{E}(a_i(t_{f+1})), \quad i = 1, \ldots, 5, \quad f = 0, \ldots, F-1, \tag{20}$$

$$\tilde{E}(a_i(t_0)) = \tilde{E}_0, \quad i = 1, \ldots, 5, \tag{21}$$

$$l(a_i(t_f)) = 2\pi, \quad i = 1, \ldots, 5, \quad f = 0, \ldots, F, \tag{22}$$

where the objective function (19) includes the integral in (15) computed according to the trapezoidal rule [1] and two penalizations terms imposed to smooth the state variables behaviors: one on the *norm* of $a_i(t_f)$, $i = 1, \ldots, 5$ with cost γ given by

$$p(t_f) = \sum_{i=1}^{5} a_i^2(t_f), \quad f = 0, \ldots, F, \tag{23}$$

and one on the *curvature* of $a_i(t_f),\ i = 1, \ldots, 5$ with cost $\mu < \gamma$, by means of the central difference approximation of the second derivative

$$k(a_i(t_f)) = \frac{\frac{a_i(t_{f+1}) - a_i(t_f)}{t_{f+1} - t_f} - \frac{a_i(t_f) - a_i(t_{f-1})}{t_f - t_{f-1}}}{t_{f+1} - t_{f-1}}\ , \qquad f = 1, \ldots, F-1, \tag{24}$$

and

$$h(t_f) = \sum_{i=1}^{5} k(a_i(t_f))^2\ , \qquad f = 1, \ldots, F-1. \tag{25}$$

In contrast with traditional interpolation, where the values at grids points (vertices) have to match some given values, we consider the value of the evolution parameters $a_i(t_f),\ i = 1, \ldots, 5$ at grids points as part of the unknowns in the optimization problem (19)-(22).

Notice that the integrals along the curve $\mathcal{C}$ of the bending energy $\tilde{E}_b(a_i(t_f))$ and of the length function $l(a_i(t_f))$, $i = 1, \ldots, 5$ in problem (19)-(22) have been computed by means of the trapezoidal rule [1] dicretizing the axis into K segments: let b be the generic integrand function, then

$$\oint_{\mathcal{C}} b \, \mathrm{d}\xi \approx \frac{2\pi}{L} \left[\frac{b(0) + b(2\pi)}{2} + \sum_{k=1}^{K-1} b(\xi_k) \right]\ . \tag{26}$$

Moreover, the double integral along the curve $\mathcal{C}$ of the writhing number Wr (5) which contributes to the mean twist energy $\tilde{E}_{tw}(a_i(t_f))$, $i = 1, \ldots, 5$, has been computed by means of the *double* trapezoidal rule: the domain rectangle

$$\mathcal{R} = \mathcal{C} \times \mathcal{C} = \{(\xi, \xi^*) : 0 \le \xi \le 2\pi, 0 \le \xi^* \le 2\pi\} \tag{27}$$

is divided into smaller sub rectangles $\{\mathcal{R}_{k,r}\}$, $k = 1 \ldots, K$ and $r = 1 \ldots, R$ obtained as the intersections of the $k-th$ subinterval in $[0, 2\pi]$ with the $r-th$ subinterval in $[0, 2\pi]$. Denoting with b the integrand function in (5), then

$$\begin{aligned} \oint_{\mathcal{C}} \oint_{\mathcal{C}} b \, \mathrm{d}\xi \mathrm{d}\xi^* \approx \frac{4\pi^2}{KR} \left(b(0,0) + b(0,2\pi) + b(2\pi,0) + b(2\pi,2\pi) + 2\sum_{k=1}^{K-1} b(\xi_k, 0) + 2\sum_{k=1}^{K-1} b(\xi_k, 2\pi) \right) + \\ + \frac{4\pi^2}{KR} \left(2\sum_{r=1}^{R-1} b(0, \xi_r) + 2\sum_{r=1}^{R-1} b(2\pi, \xi_r) + 4\sum_{r=1}^{R-1} \sum_{k=1}^{L-1} b(\xi_k, \xi_r) \right)\ , \end{aligned} \tag{28}$$

also called the *four-corners method*.

Problem (19-22) is then solved in the case of single coil formation ($n_1 = 1$, $n_2 = 2$ in eq. (3)) with length function:

$$l(a_i(t)) = \int_{\mathcal{C}} \sqrt{\sin^2(\xi)(a_1(t) + 4a_2(t)\cos(\xi))^2 + (a_3(t)\cos(\xi) + 2a_4(t)\cos(2\xi))^2 + a_5^2(t)\cos^2(\xi)} \mathrm{d}\xi\ ,$$

and bending energy $\tilde{E}_b$:

$$\tilde{E}_b = \int_{\mathcal{C}} [12\cos(\xi)\left(a_1^2 a_3 a_4 + a_1 a_2\left(a_3^2 + 8a_4^2 + a_5^2\right) + 8a_2^2 a_3 a_4\right) +$$
$$3\cos(2\xi)\left(a_4^2\left(a_1^2 - a_5^2\right) + 6a_1 a_2 a_3 a_4 + 5a_2^2\left(a_3^2 + a_5^2\right)\right) + 2a_1^2 a_3^2 - 4a_1^2 a_3 a_4\cos(3\xi) - 6a_1^2 a_4^2\cos(4\xi) +$$
$$+ a_2^2 a_4^2\cos(6\xi) + 10a_1^2 a_4^2 + 2a_1^2 a_5^2 + 4a_1 a_2 a_3^2\cos(3\xi) - 2a_1 a_2 a_3 a_4\cos(6\xi) + 48a_1 a_2 a_3 a_4 +$$
$$-32a_1 a_2 a_4^2\cos(3\xi) + 4a_1 a_2 a_5^2\cos(3\xi) + 6a_2^2 a_3^2\cos(4\xi) + a_2^2 a_3^2\cos(6\xi) + 10a_2^2 a_3^2 + 32a_2^2 a_3 a_4\cos(3\xi) +$$
$$128a_2^2 a_4^2 + 6a_2^2 a_5^2\cos(4\xi) + a_2^2 a_5^2\cos(6\xi) + 10a_2^2 a_5^2 - 6a_4^2 a_5^2\cos(4\xi) - a_4^2 a_5^2\cos(6\xi) + 10a_4^2 a_5^2]/$$
$$[2\big(\sin^2(\xi)(a_1 + 4a_2\cos(\xi))^2 + (a_3\cos(\xi) + 2a_4\cos(2\xi))^2 + a_5^2\cos^2(\xi)\big)^{5/2}]\mathrm{d}\xi \qquad (29)$$

approximated according to eq. (26). According to the critical twist value (14) we set $Lk = 3$ such that the mean twist energy $\tilde{E}_{tw}$ becomes:

$$\tilde{E}_{tw}(a_i(t)) = (3 - Wr(a_i(t)))^2 \qquad (30)$$

with $\chi = 1$. Notice that, to avoid the singularity in the integrand function of Wr for $\xi \to \xi^* + 2k\pi$, $(k = 0, 1)$, we set its value at the four vertices of the domain integration $\mathcal{R}$, equal to zero.

The initial ($t = 0$) configuration in eq. (3) is chosen to be a circle of unitary radius:

$$\mathbf{X} = \mathbf{X}(\xi, 0) \ : \quad \begin{cases} x = \cos(\xi) \\ y = \sin(\xi) \\ z = 0 \end{cases}, \qquad (31)$$

obtained by setting

$$(a_1(0), a_2(0), a_3(0), a_4(0), a_5(0)) = (1, 0, 1, 0, 0), \qquad (32)$$

with associated initial deformation energy $\tilde{E}_0 = 10$.

5.1 Splines functions for kinematics

Time evolution functions $a_i(t)$, $i = 1, \ldots, 5$ in problem (19)-(22) are described by means of piecewise polynomial transformations based on cubic B-splines and Hermite splines functions. We briefly recall their definitions and main properties.

5.1.1 Kinematics by cubic B-spline functions

A *B-spline function* is a generalization of a *Beziér curve* [7].
Let T be a nondecreasing sequence of knots $t_w \in [t_0, t_{fin}] = [0, 1]$ known as the *knot vector*:

$$T = \{t_0, t_1, \ldots, t_m\} \ . \qquad (33)$$

A B-spline of degree n, is a parametric curve composed of a linear combination of basis B-splines $b_w^n(t)$ of degree n with $w = 0, \ldots, m-n-1$. Kinematic functions $a_i(t)$ can be then described as follows

$$a_i(t) = \sum_{w=0}^{m-n-1} P_{i,w} b_w^n(t), \quad i = 1, \ldots, 5, \tag{34}$$

where $P_{i,w}$, $w = 0, \ldots, m-n-1$, $i = 1, \ldots, 5$ are called *control points* or *de Boor points* forming a convex hull; the basis B-spline $b_w^n(t)$ are defined using the *Cox-de Boor recursion formula*:

$$b_w^0(t) = \begin{cases} 1 & \text{if } t_w < t < t_{w+1} \text{ and } t_w < t_{w+1} \\ 0 & \text{otherwise} \end{cases}$$

$$b_w^j(t) = \frac{t - t_w}{t_{w+j} - t_w} b_w^{j-1}(t) + \frac{t_{w+j+1} - t}{t_{w+j+1} - t_{w+1}} b_{w+1}^{j-1}(t), \qquad j = 1, \ldots, n\ .$$

They satisfy the following properties:

- $b_w^j(t)$ is a degree j polynomial in t;
- for all w, j and t, $b_w^j(t)$ is non negative;
- $b_w^j(t)$ is a non-zero polynomial on $[t_w, t_{w+j+1})$;
- on any span $[t_w, t_{w+1})$ at most $j+1$ degree j basis functions are non zero, namely: $b_{w-j}^j(t), b_{w-j+1}^j(t), b_{w-j+2}^j(t) \ldots, b_w^j(t)$;
- the sum of all non-zero degree j basis functions on span $[t_w, t_{w+1})$ is 1;
- if the number of knots is $m+1$, the degree of the basis functions is j, and the number of degree j basis function is $p+1$, then $m = p + j + 1$;
- basis function $b_w^j(t)$ is a composite curve of degree j polynomials with joining points at knots in $[t_w, t_{w+j+1})$;
- at a knot of multiplicity k, basis function $b_w^j(t)$ is C^{j-k} continuous.

In the implementation we will consider a special case of non-periodic B-spline where the first $n+1$ knots are equal to zero and the last $n+1$ knots are equal to one forcing the curve to pass by them, and the internal knots $t_{n+1}, \ldots, t_{m-n-1}$ corresponding to the grid points $t_0, \ldots, t_{fin}$. Figure 3 represents cubic B-spline basis $b_w^3(t)$, $w = 0, \ldots, 6$ through the grid points $\{0, 1/4, 1/2, 3/4, 1\}$ over $[0, 1]$.

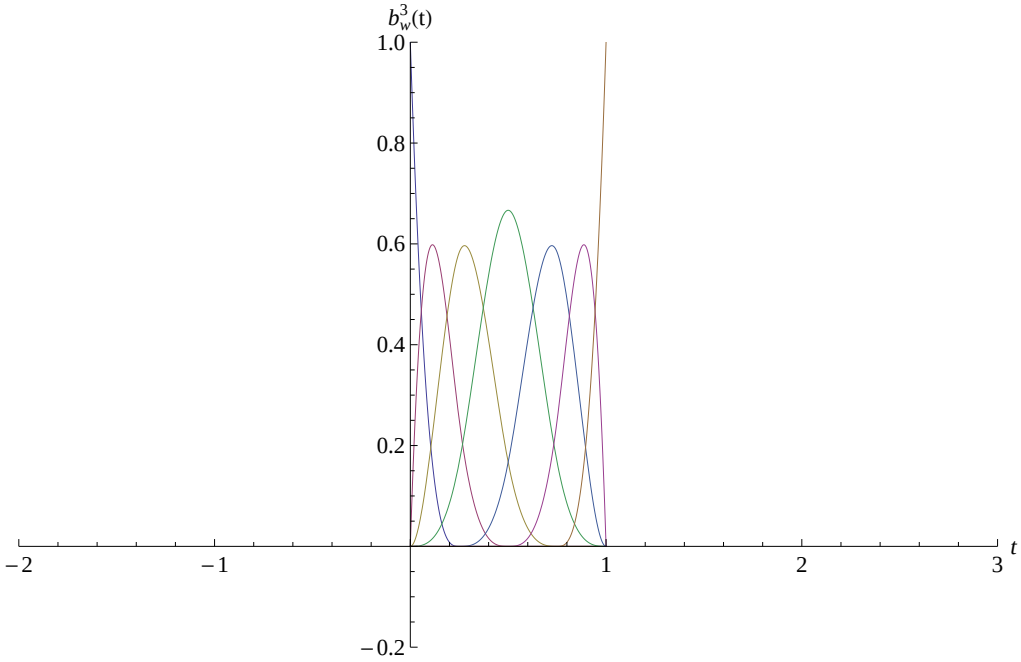

Figure 3: B-splines basis $b_w^3(t)$, $w = 0, \ldots, 6$ of degree 3 over $[0, 1]$ through the knot vector $T = \{0, 0, 0, 0, 1/4, 1/2, 3/4, 1, 1, 1, 1\}$.

5.1.2 Kinematics by cubic hermite spline functions

The other representation adopted is given by *cubic Hermite spline* [7], a particular class of third-degree spline interpolation with each polynomial of the spline in Hermite form. The Hermite form consists of two control points and two control tangents for each polynomial. Given a nondecreasing sequence of points $t_f \in [t_0, t_F]$, the sub-interval (t_f, t_{f+1}) is normalized to $(0, 1)$ via

$$x = \frac{t - t_f}{t_{f+1} - t_f}$$

and the restriction of the function $a_i(t)$ is a polynomial $a_i^f : [t_f, t_{f+1}] \to \mathbb{R}$ represented as follows:

$$a_i^f(t) = a_{i,00}^{(f)} h_{00}(x) + a_{i,01}^{(f)} h_{01}(x) + a_{i,10}^{(f)} (t_{f+1} - t_f) h_{10}(x) + a_{i,11}^{(f)} (t_{f+1} - t_f) h_{11}(x) \,, \quad f = 0, \ldots, F-1, \tag{35}$$

where

$$\begin{cases} h_{00}(x) &= 2x^3 - 3x^2 + 1 \\ h_{01}(x) &= -2x^3 + 3x^2 \\ h_{10}(x) &= x^3 - 2x^2 + x \\ h_{11}(x) &= x^3 - x^2 \end{cases}$$

are Hermite basis functions and $a_{i,00}^{(f)}$ and $a_{i,01}^{(f)}$ respectively the stating and final point with their derivatives $a_{i,10}^{(f)}(t_{f+1}-t_f)$ and $a_{i,11}^{(f)}(t_{f+1}-t_f)$ chosen to be continuously differentiable to the first order at the interior points t_f, $f=1,\ldots,F-1$:

$$a_{i,01}^{f}(t_f) = a_{i,00}^{f+1}(t_f)\ , \tag{36}$$

$$a_{i,11}^{f}(t_f) = a_{i,10}^{f+1}(t_f)\ . \tag{37}$$

The condition of continuity of the second order derivatives will be imposed adding an extra constraint in the model (19)-(22).

6 Numerical results

Problem (19)-(22) in the case of single coil formation, has been solved under Mathematica 8.0 environment by means of the *NMinimize* function which implements several algorithms for finding constrained global optima. The optimization methods available are: the *Nelder Mead Method*, a direct search method which do not use derivative information, *Differential Evolution* and *Simulated Annealing*, two simple stochastic function minimizers and the *Random Search Algorithm*, which generates a population of random starting points and uses a local optimization method from each of them. *NMinimize* picks which method to use based on the type of problem and in our case Nelder-Mead has been used. For a function of n variables, the algorithm maintains a set of $n+1$ points forming the vertices of a polytope in n-dimensional space. This method is often termed the "simplex" method, which should not be confused with the well-known simplex method for linear programming. NelderMead generates a new test position by extrapolating the behavior of the objective function measured at each test point arranged as a simplex. The algorithm then chooses to replace one of these test points with the new test point and so the technique progresses. The simplest step is to replace the worst point with a point reflected through the centroid of the remaining n points. If this point is better than the best current point, then we can try stretching exponentially out along this line. On the other hand, if this new point isn't much better than the previous value, we shrink the simplex towards a better point. There are several stopping criteria that have been proposed for this algorithm: Nelder and Mead suggest halting the algorithm when the standard error of the function values fall below some threshold value (see [15]).

Finding a global optimum can be arbitrarily difficult, even without constraints, and so the methods used may fail. For this reason we have also solved the problem by means of a local optimization software package under Mathematica *Knitro release 7*, which finds local solutions of large-scale, continuous nonlinear problems. We take as starting conditions the solutions obtained with the Nelder-Mead method and solve the problems implementing the *Interior Point Method* algorithm. In the following computational experiments we set $\gamma = 0.001$, $\mu = 0.1$, the time interval $[t_0, t_{fin}] = [0,1]$ is divided into 4 sub-intervals of constant width 0.25 and the single and double integrals in space for the computation of the length function and deformation energy, respectively by dividing the curve into $K = 10$ segments and the domain $\mathcal{R} = \mathcal{C} \times \mathcal{C}$ into $KR = 100$ sub rectangles. Problem (19)-(22) is solved in terms of

B-spline representation with 30 free variables given by the control points $P_{i,w}$, $w = 1, \ldots, 6$, $i = 1, \ldots, 5$ in (34) and initial ($w = 0$) conditions

$$(P_{1,0}, P_{2,0}, P_{3,0}, P_{4,0}, P_{5,0}) = (1, 0, 1, 0, 0) \ . \tag{38}$$

Notice that the constraints (20)-(22) are enforced every 0.1 time constant width instead of 0.25; consequently the problem is composed by 10 nonlinear equalities and 10 nonlinear inequalities. The number of nonzeros in Jacobian are 365 and in Hessian 465. The interior point method from Knitro needed 30 iterations to solve this problem, 285 coniugate gradient iterations, 112 function evaluations, 31 gradient evaluations and 30 Hessian evaluations. Final absolute feasibility error is 1.01e-009 and final absolute optimality error 3.31e-007.

The execution time was 3181.66 seconds by means of the Nelder-Mead method and only 10.34 under the software package Knitro using a personal computer VAIO Intel Core i5 processor, Windows 7 Professional (64-bit) S Series, 4GB Memory.

Optimal objective function value is 9.53, optimal control points variables are reported in Table 1 and optimal B-spline kinematic solutions plotted in Figures 4-12.

$P_{i,w}$	$i = 1$	$i = 2$	$i = 3$	$i = 4$	$i = 5$
$w = 0$	1	0	1	0	0
$w = 1$	0.908	0.061	0.98	-0.012	0.594
$w = 2$	0.908	-0.241	0.984	-0.242	0.252
$w = 3$	0.659	-0.258	0.811	-0.291	0.748
$w = 4$	0.290	-0.151	0.611	-0.396	1.038
$w = 5$	0.396	-0.462	0.373	-0.320	0.839
$w = 6$	0.101	-0.166	0.331	-0.400	1.121

Table 1: Optimal solutions of problem (19)-(22) solved in the case of single coil formation by means of the cubic B-spline function representation.

Figure 5 shows the total elastic energy $\tilde{E}(t)$ versus time t associated to the kinematics solution depicted in Figure 12. Black dots mark the grid points where the constraint (20) is enforced: the monotonic decreasing behavior is satisfied and as expected the largest value that is going to be relaxed is $\tilde{E}(0) = 10$. Contributions to the total deformation energy from bending and mean twist components are plotted in Figure 6(a)-(b): $\tilde{E}(b)$ grows from $\tilde{E}(0) = 1$ associated to the initial circular configuration of unitary radius to 3 in the final state. Conversely the mean twist energy $\tilde{E}_{tw}(t)$ decreases from $\tilde{E}_{tw}(0) = 9$ (since $Wr(0) = 0$) beeing related to the change in filament writhing.

Inextensibility constraint (22) is also satisfied as we can see from Figure 7 which shows the filament length function $l(t)$ versus time $t \in [0, 1]$. As before, black dots mark the grid points where the constraint (22) is enforced. In Figure 8 the behaviors of Lk, $Wr(t)$ and $Tw(t)$ are shown: Lk is constant and equal to 3 as expected and as t increases, the twist $Tw(t)$ is converted in writhe $Wr(t)$ according to (9). The coiling induced by filament folding

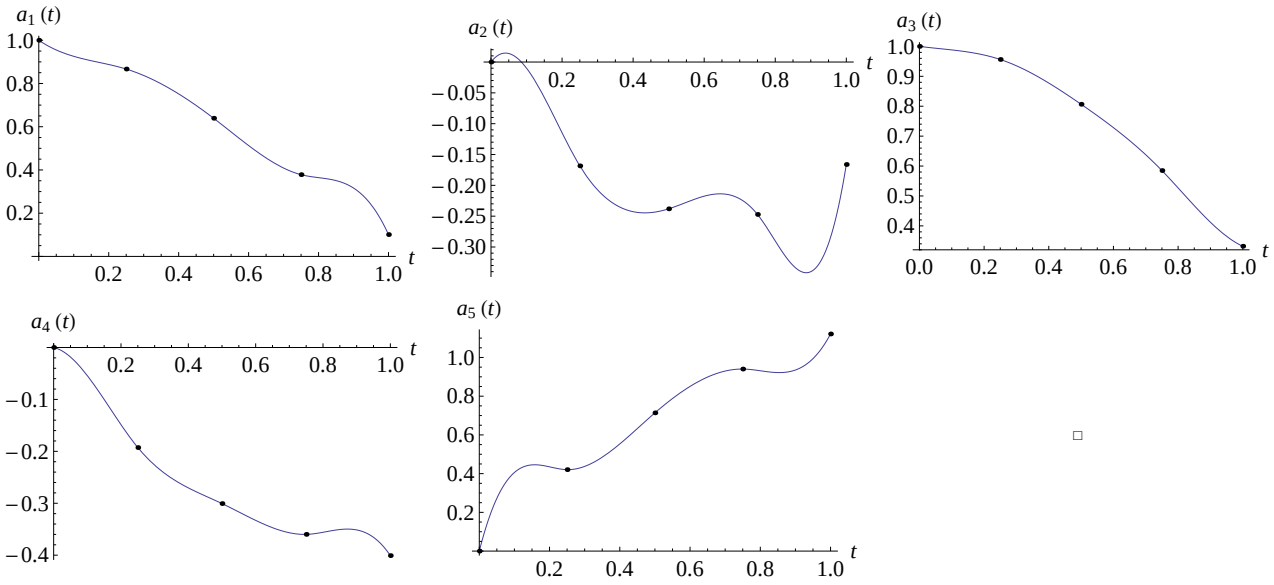

Figure 4: Kinematic B-spline solutions $a_i(t)$, (first line case $i = 1, 2, 3$, second line case $i = 4, 5$) plotted versus time $t \in [0, 1]$, with $F = 4$ sub-intervals.

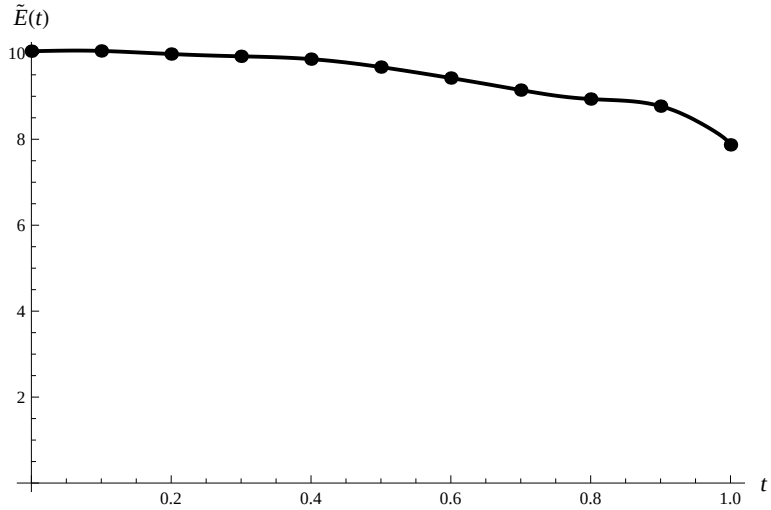

Figure 5: Total elastic energy $\tilde{E}(t)$ plotted versus time. Black dots mark the grid points where the constraint (20) is enforced.

is also measured by the growth in total curvature $\mathcal{K}(t)$ plotted in Figure 9 due to average curvature associated with the process. Both $\mathcal{K}(t)$ and $Wr(t)$ increase in time. Contributions of total twist $Tw(t)$ from normalized total torsion $\mathcal{T}$ and intrinsic twist $\mathcal{N}$ according to the decomposition (8) are plotted in Figure 10, showing the conversion of one of the three initial units of intrinsic twist (since initial conditions are given by $\mathcal{T} = 0$ and $\mathcal{N} = 3$) to total torsion

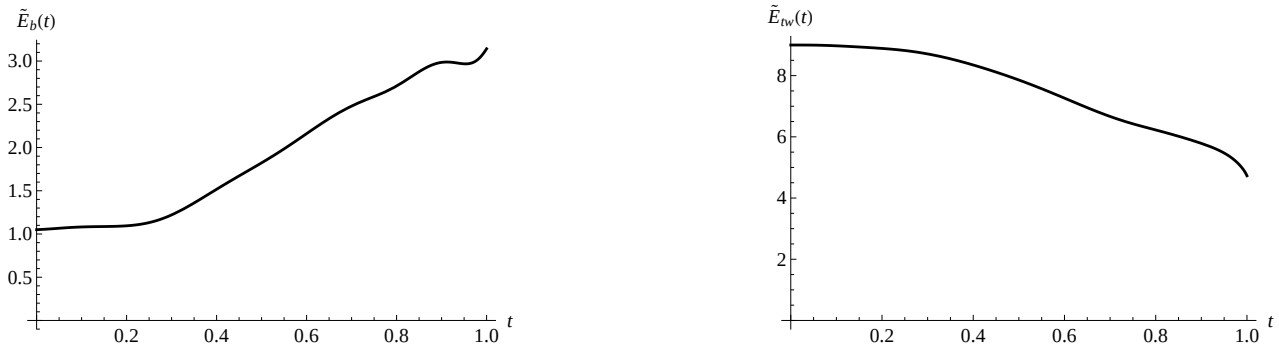

(a) (b)

Figure 6: (a) Bending energy $\tilde{E}_b(t)$ and (b) mean twist energy energy $\tilde{E}_{tw}(t)$ plotted versus time.

at $t = 0.3$. The conversion is associated to the passage through an inflexional configuration (see Figure 11) characterized by the occurrence of a point on the curve with zero curvature and local change of concavity of the curve. At the point of inflexion the torsion is singular but the singularity is integrable and the contribution from the integral of the total torsion through the inflexional state involves a jump $[\mathcal{T}] = 1$ in total torsion that must be compensated by an equal and opposite jump in the intrinsic twist $\mathcal{N}$ so that Tw remains a smooth function in space and time (see [14] and [12] for a detailed analysis). All the graphics described refer to the kinematics solution depicted in Figure 12 which shows the evolution of the initial circular configuration towards an energetically preferable final state. Notice that the non-constant behavior of Wr and Tw at the end of the time interval considered, means that the curve at $t = 1$ has not reach yet an equilibrium configuration. We expect that leaving the curve to evolve for $t > 1$ it will reach a planar equilibrium configuration associated to the figure-eight (see [24]).

Convergence has been tested in space and time, by modifying the number of discretization points and the size of the time step. Convergence in time has been tested by ranging the time step from 0.05 to 0.5: notice that for an increasing number of discretization points (and consequently larger number of variables), the solvers used does poorly and the solution variables show a random behavior. Future research will plan to develop a specific solver addressed for this problem. Convergence in space has been tested by dividing the curve from 5 to 30 segments. Convergence for different values of the smoothing parameters $\gamma \in [0, 0.1]$ and $\mu \in [0, 0.1]$ has been also tested showing a regular behavior of the solution choosing $\mu > \gamma$ with $\mu = 0.1$.

For the sake of comparison, problem (19)-(22) has been also solved in terms of Hermite-spline representation (35) with 45 free variables given by the control points and control tangents

$$a^{(f)}_{i,00}, a^{(f)}_{i,01}, a^{(f)}_{i,10}, a^{(f)}_{i,11} \ , \qquad f = 0, \ldots, 3, \quad i = 1, \ldots, 5 \ ,$$

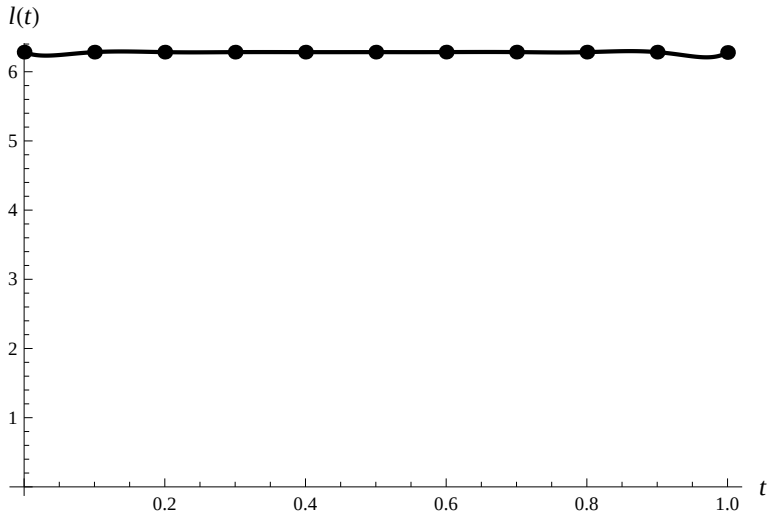

Figure 7: Filament length function $l(t)$ versus time. Black dots mark the grid points where the constraint (22) is enforced.

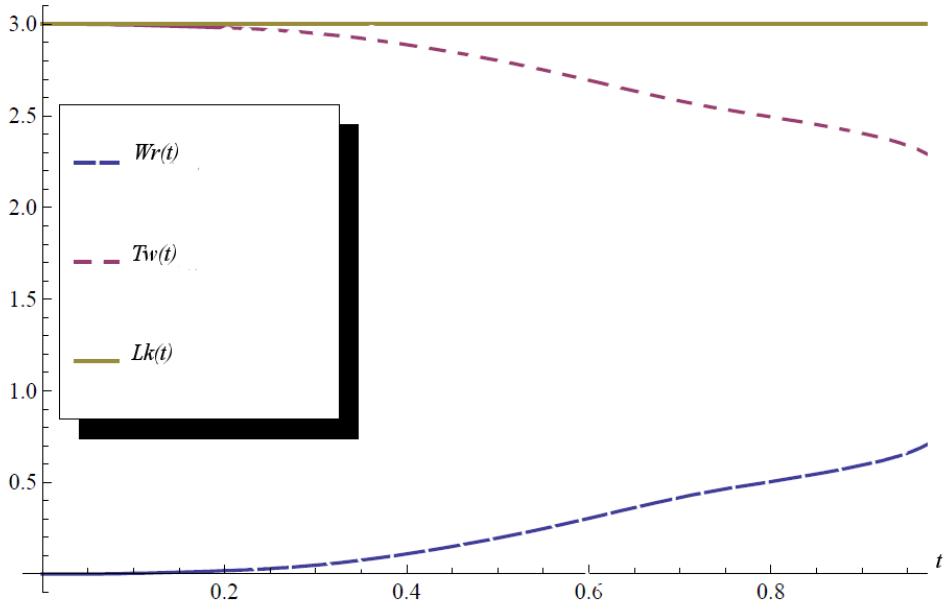

Figure 8: Evolution of $Wr(t)$, $Tw(t)$ and Lk versus time.

satisfying conditions (36)-(37) and initial ($t = 0$) condition as follows:

$$\left(a^{(0)}_{1,00}, a^{(0)}_{2,00}, a^{(0)}_{3,00}, a^{(0)}_{4,00}, a^{(0)}_{5,00}\right) \;=\; (1,0,1,0,0)\ . \tag{39}$$

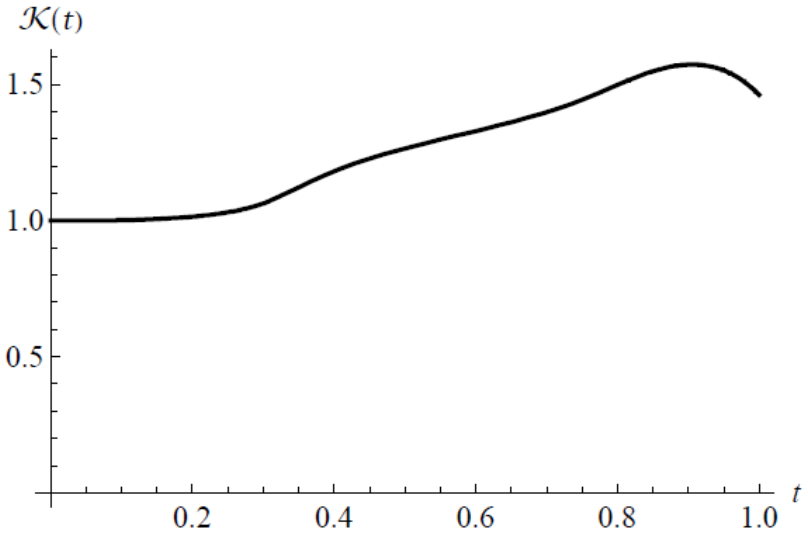

Figure 9: Evolution of total curvature $\mathcal{K}(t)$ versus time.

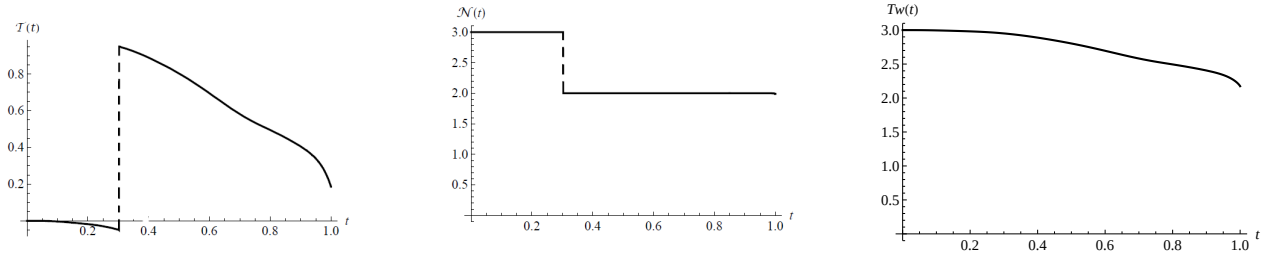

(a) (b) (c)

Figure 10: (a) Normalized total torsion $\mathcal{T}(t)$ and (b) normalized intrisinc twist $\mathcal{N}(t)$ versus time. Note that at the passage through the inflexional configuration at $t = 0.3$ the discontinuities in $\mathcal{T}$ and $\mathcal{N}$ compensate so $Tw(t) = \mathcal{T}(t) + \mathcal{N}(t)$ (c) is still a smooth function in space and time.

Constraints on the continuity of the second order derivatives have been also included. Because of the larger dimension of problem with the cubic Hermite spline representation in terms of variables and constraints, we performed the analysis in terms of the more convenient B-spline representation.

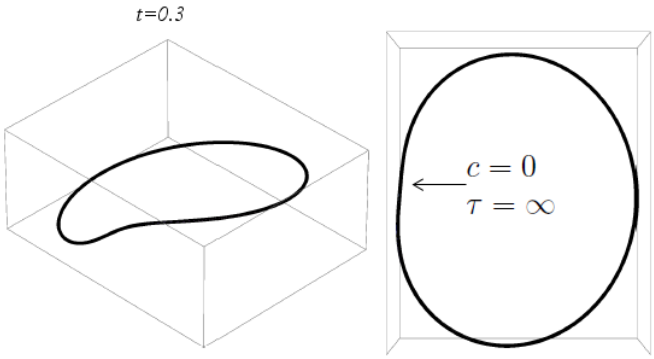

Figure 11: Side and top view of the occurrence at $t = 0.3$ of an inflexional configuration characterized by point on the curve with zero curvature.

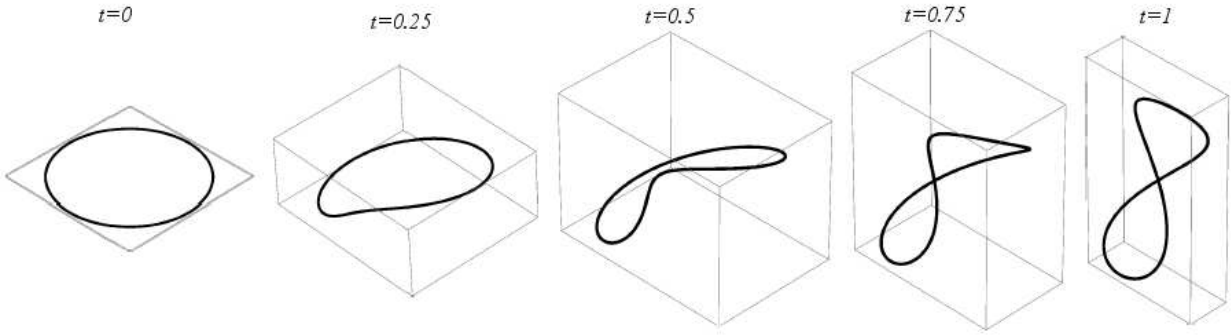

Figure 12: Side view of one coil formation solution by means of the cubic B-spline interpolation method depicted in $[t_0, t_{fin}] = [0, 1]$ with time step $q = 0.25$.

7 Conclusions

In this paper kinematics of supercoiling of closed filaments as solutions of the elastic energy minimization are proposed. The model presented is applied to the case of single coil formation and it requires a monotonic decreasing behavior in time of the elastic energy in terms of bending and twisting contributions; it includes constraints to ensure fixed contour length of the filament and prescribed initial condition on critical twist value to generate the coiling. Time evolution functions are described by means of piecewise polynomial transformations based on cubic B-spline spline functions considering their values at grids points as the unknowns in a non-linear optimization problem. This represents the main contribution of the paper with respect to the companion articles [12] and [17] where time dependence has been prescribed to

investigate geometric features associated with the coiling process.

The results show the energetic exchange between the initial circle and the final figure-eight interwound associated with conversion of mean twist energy into bending energy. Geometric characteristics of the filament evolution such as writhing number, normalized total curvature and twist in terms of its contributions from normalized total torsion and intrinsic twist have been analyzed in relation to the passage through an inflexional configuration involving a localized distorsion of the filament fibers.

This mechanism has physical relevance in the context of elastic rod theory [10], where the deformation process is mechanically justified by a writhing instability [26] characterized by an instability of the elastic ring which start writhing out of the plane for sufficiently high twist.

Future research will plan to develop a specific solver addressed for this problem able to solve a large scale optimization problem associated to multiple coils and knots formation, relevant in biological systems [23].

The model proposed find useful applications in modeling DNA supercoiling of nucleosome and viral spooling, where there is strong connection between high coiling and energy localization [2].

References

[1] Atkinson, Kendall E. (1989) An introduction to Numerical Analysis, New York.

[2] Arsuaga, J., Tan, R.K.Z., Vazquez, M., Sumners, D.W. & . Harvey S.C (2002) Investigation of viral DNA packaging using molecular mechanics models. *Biophysical Chemistry* **101**, 475–484.

[3] Benham, C.J. (1989) Onset of writhing in circular elastic polymers. *Phys. Rev. A* **39**, 2582–2586.

[4] Bauer, W.R., Crick, F.H.C. & White J.H. (1980) Supercoiled DNA. *Scientific American* **243**, 100–113.

[5] Călugăreanu, G. (1961) Sur les classes d'isotopie des nœuds tridimensionnels et leurs invariants. *Czechoslovak Math. J.* **11**, 588–625.

[6] Cozzarelli, N.R. & Wang, J.C. (1990)(Editors) *DNA Topology and its Biological Effects.* Cold Spring Harbor Laboratory Press, Cold Spring Harbor, NY.

[7] De Boor, C. (1978) *A practical guide to splines, Applied Mathematical Sciences,* Vol. 27 (New York: Springer Verlag).

[8] Fuller, F.B. (1971) The writhing number of a space curve. *Proc. Natl. Acad. Sci. U.S.A.* **68**, 815–819.

[9] Goriely, A. (2006) Twisted elastic rings and the rediscoveries of Michell's instability. *L. Elasticity* **84**, 281–299.

[10] Klapper, I. (1996) Biological applications of the dynamics of twisted elastic rods. *J. Comp. Phys.* **125**, 325–337.

[11] LeBret, M. (1984) Twist and writhing in short circular DNA according to first-order elasticity. *Biopolymers* **23**, 1835–1867.

[12] Maggioni, F & Ricca, R.L. (2006) Writhing and coiling of closed filaments. *Proc. R. Soc. A* **462**, 3151–3166.

[13] Michell, J.H. (1889–1990) On the stability of a bent and twisted wire. *Messenger of Math.* **11**, 181–184.

[14] Moffatt, H.K. & Ricca, R.L. (1992) Helicity and the Călugăreanu invariant. *Proc. R. Soc. Lond.* A **439**, 411–429.

[15] Nocedal, J. & Wright S.J. (1999) Numerical Optimization, Springer Series in Operations Research.

[16] Ricca, R.L. (1995) The energy spectrum of a twisted flexible string under elastic relaxation. *J. Phys.* A: *Math. Gen.* **28**, 2335–2352.

[17] Ricca, R.L. & Maggioni, F. (2008) Multiple folding and packing in DNA modeling. *Comp. & Maths. with Appl.*, **55**, 1044–1053.

[18] Schlick, T. (1995) Modeling Superhelical DNA: Recent Analytical and Dynamical Approaches. *Curr. Opin. Struct. Biol.* **5**, 245.

[19] Schlick, T. & Olson W. (1992) Supercoiled DNA energetics and dynamics by computer simulation. *J. Mol. Biol.* **223**, 1089–1119.

[20] Starosin, E. (1996) Three-dimensional shapes of looped DNA. *Meccanica* **31**, 235–271.

[21] Starosin, E. (2004) Symmetric equilibria of a thin elastic rod with self-contacts *Phil. Trans. R. Soc. Lond. A*, **362** 1317–1334.

[22] Stasiak, A. (1996) Circular DNA. In *Large Ring Molecules* (ed. J.A. Semlyen), John Wiley & Sons Ltd, 43–97.

[23] Sumners, D.W.(2009) Random Knotting: Theorems, Simulations and Applications. In: Lectures on Topological Fluid Mechanics, Lecture Notes in Mathematics **187**, Springer, (Ed.) R.L. Ricca. 201–231.

[24] Wadati, M. & Tsuru, H. (1986) Elastic model of looped DNA. *Physica 21D*, 213–226.

[25] White, J.H. (1969) Self-linking and the Gauss integral in higher dimensions. *Amer. J. Math.* **91**, 693–728.

[26] Zajac, E.E. (1962) Stability of two planar loop elasticas. *ASME J. Applied Mechanics*, **29**, 136–142.